Supplementary Information

Pool Boiling Performance of Water and Self-Rewetting Fluids on Hybrid Functionalized Aluminum Surfaces

Matic Može[a,*], Viktor Vajc[b], Matevž Zupančič[a], Radek Šulc[b], Iztok Golobič[a]

[a] *Faculty of Mechanical Engineering, University of Ljubljana, Aškerčeva 6, 1000 Ljubljana, Slovenia*

[b] *Faculty of Mechanical Engineering, Czech Technical University in Prague, Technická 4, 160 00 Prague 6, Czech Republic*

Corresponding authors:

* E-mail: matic.moze@fs.uni-lj.si, +396 1 4771 309 (M. Može)

Table of Contents

S1. Numerical validation of the dynamic measurement method

Approach to numerical simulations

A series of numerical simulations was performed to validate that the dynamic method of boiling curve measurements provides accurate results in comparison with commonly employed steady-state measurements. Specifically, we set out to evaluate the difference between the results that are obtained based on transient temperature measurements in the sample and the actual values of heat transfer parameters (mainly heat flux and superheat) on the boiling surface, which were obtained from the simulation. The purpose of the validation is to show that very slow changes in heat flux (< 0.2 kW m^{-2} s^{-1} in the natural convection regime and < 2.5 kW m^{-2} s^{-1} in the nucleate boiling regime) do not cause deviations from steady-state measurements while allowing for faster evaluation boiling performance. Similar simulations were already performed in the past for another experimental setup for pool boiling performance evaluation and are included in the Supplementary Material of [1].

Within the current simulations, we numerically investigated the behavior of the temperature distribution in the cylindrical sample with the same geometry as in our experiments. Like during measurements and data reduction, only 1D conduction along the sample towards the boiling surface is considered while the heat losses through the lateral surface of the sample are neglected (adiabatic wall condition). Spatially uniform conditions were considered at the remaining two boundaries. Under these conditions, the general three-dimensional heat conduction problem can be simplified to a one-dimensional, transient heat transfer case:

$$\frac{\partial T}{\partial t} = \frac{k}{\rho c_p}\frac{\partial^2 T}{\partial x^2} \qquad\qquad (S1)$$

In Eq. S1, ρ denotes the density, c_p the specific heat and k the thermal conductivity of the sample.

We solved this simplified partial differential equation by adopting a finite volume approach and a convenient implicit time integration scheme. The calculation has been carried out by assuming constant density and specific heat within the computational domain. However, we included the temperature dependence of the thermal conductivity in accordance with the following equation (k in W m^{-1} K^{-1}, T in °C):

$$k(T) = -0.0001165T^2 + 0.07486T + 198.81 \qquad\qquad (S2)$$

Under the aforementioned assumptions, the discretized form of the energy balance for a one-dimensional control volume reads:

$$\frac{T_i{}^{n+1}-T_i{}^n}{\Delta t} = -\frac{k_{i,w}}{\rho c_p}\frac{\left(T_i{}^{n+1}-T_{i-1}{}^{n+1}\right)}{\Delta x^2} - \frac{k_{i,e}}{\rho c_p}\frac{\left(T_i{}^{n+1}-T_{i+1}{}^{n+1}\right)}{\Delta x^2} \qquad (S3)$$

In the latter equation, n is the index of solved time layer and i is the ordinal index of solved cell. The values of $k_{i,w}$ and $k_{i,e}$ are obtained by ensuring the continuity of heat flux between

adjacent nodes in the domain. Considering a uniform spacing between the nodes (see the sketch on figure S1.1) one gets:

$$k_{i,w} = 2\frac{k_i k_{i-1}}{k_i + k_{i-1}} \qquad k_{i,e} = 2\frac{k_i k_{i+1}}{k_i + k_{i+1}} \tag{S4}$$
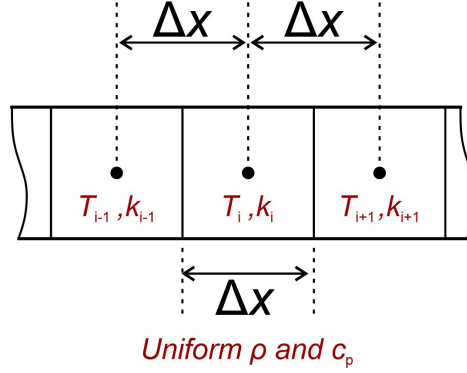
Figure S1.1. Sketch of an elementary cell of the one-dimensional domain.

Time-dependent temperature boundary condition was used at the bottom of the considered geometry, representing the point where the bottommost thermocouple is located during measurement. Temperatures obtained during measurement of pool boiling performance obtained on three different samples within this study (REF, A5 and A5H) were used. Since the rates of temporal temperature change are different during natural convection, nucleate boiling and CHF onset, the measured data was split into three intervals and polynomials of different degrees were used to approximate the measured trends. Each polynomial is defined using relative time (starting with zero at the beginning of the given time interval). Continuity during transition between neighboring intervals is realized through appropriate constants. The exact polynomials used for each surface are provided together with the results in the following subsections.

A heat transfer coefficient boundary condition was imposed on the other end of the considered domain, where heat transfer from the boiling surface to the fluid takes place during the measurement. Measured, time-dependent values of the heat transfer coefficient were used to impose the boundary conditions. As with the temperature boundary condition, the measurements were split into three intervals based on significantly different heat transfer behavior during natural convection, nucleate boiling and CHF onset. A constant heat transfer coefficient value was used for the natural convection regime (obtained as an average value based on measurements on a given sample) and a polynomial was used to describe the heat transfer coefficient behavior in the nucleate boiling regime. The CHF onset was modelled with an exponential decay function.

Time dependencies of heat transfer coefficient and bottom temperature, which were used as boundary conditions, were synchronized to match the measurement results. As there is a

possible (yet very small) delay between the bottom temperature and corresponding heat transfer coefficient due to the transient nature of the measurement method, another simulation was performed where Rohsenow's correlation [2] was used to calculate the heat transfer coefficient based on the current (i.e., most up-to-date) surface superheat to further validate results of simulations.

All simulations were carried out with 1000 internal nodes ($\Delta x = 0.0153$ mm) and with a time step of 0.1 s. Transitions from the natural convection to nucleate boiling and from nucleate boiling towards CHF onset occurred when a specific bottom temperature was reached, which was known in advance from measured data. The simulation was terminated 5 seconds after reaching the CHF.

For each simulation, the discretization scheme of the computational domain in shown together with the time dependence of both boundary conditions. Equations for heat transfer coefficient and bottom temperature implemented as boundary conditions are also provided. Following subplots are included in the figures showing each set of simulation results:

a) The temporal dependence of temperature at four monitoring locations (location of the first thermocouple at the bottom of the sample 15.3 mm below the boiling surface, location of the second and third thermocouple at a distance of 5 mm and 10 mm from the bottom thermocouple, respectively, and the boiling surface).

b) Comparison of two boiling curves: one is plotted directly from the simulation results at the surface of the sample ($x = L$), while the other is calculated as during the measurements from the temperature difference between the bottom of the sample and location of the uppermost thermocouple ($x = 10$ mm). The protocol of heat flux calculation and surface temperature extrapolation is the same as described within the manuscript. Standard measurement uncertainty is also provided to give a reference for the comparison of the magnitude of the deviation between the two boiling curves.

c) The difference between boiling surface temperature as simulated at $x = L$ and as extrapolated versus time with a highlighted region of nucleate boiling, which is of interest for this study.

d) The difference between calculated and simulated heat flux (solid line) together with the comparison of simulated heat flux at the bottom and the top of the sample (dashed line). Additionally, the temporal dependence of heat flux change rate (i.e., the change of heat flux over time, which is the basis of the dynamic measurement method) is plotted with respect to the right y-axis.
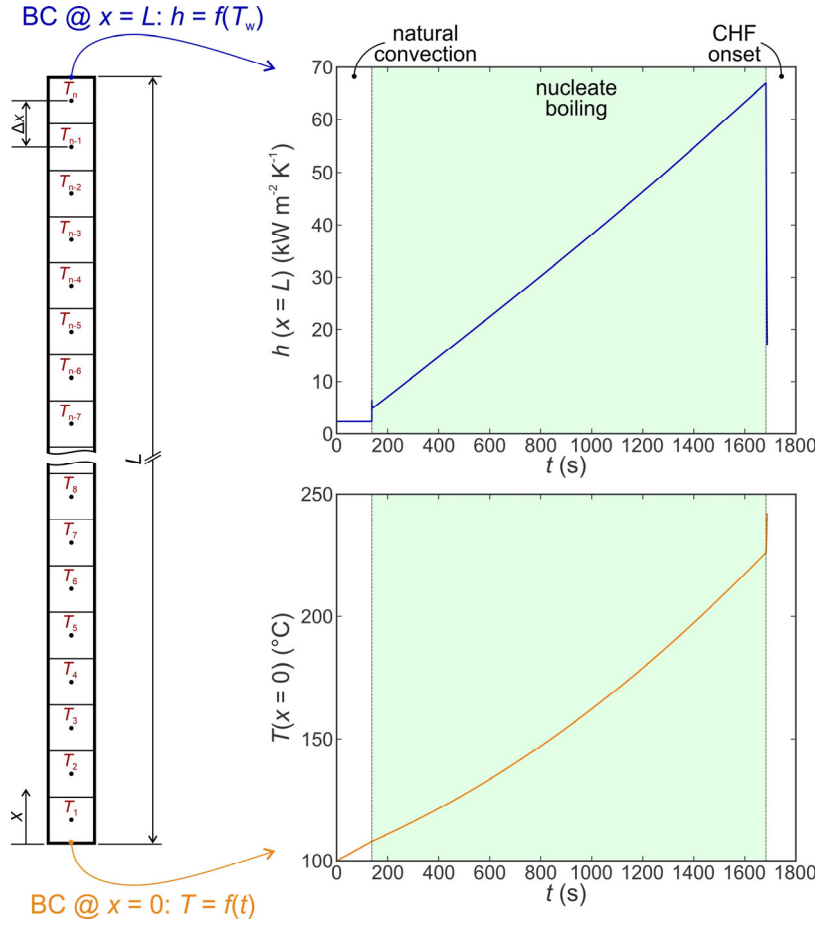
Simulation on the reference sample with Rohsenow's correlation

The first simulation was performed using the bottom temperature data recorded during experiments on an untreated reference sample. The heat transfer coefficient in the natural convection regime was determined experimentally, while the nucleate boiling heat transfer coefficient was determined based on the most current value of surface superheat using Rohsenow's correlation. For the latter, thermophysical properties were determined using REFPROP 10.0 for saturated pure water at 101.325 kPa. The values of the coefficient and the exponent in Rohsenow correlation were $C_{sf} = 0.0153$ and $n = 1$. The boundary conditions are summarized in Table S1.1, where t_{rel} denotes relative time within each interval (starting from zero). The exponential decay function used to model the heat transfer coefficient during the CHF onset considers the highest heat transfer coefficient obtained in the previous interval (i.e., at the end of the nucleate boiling regime), which is denoted as $h_{max,NB}$ and had the value of 66.95 kW m^{-2} K^{-1}.

Table S1.1. Boundary conditions for the simulation on the reference sample using Rohsenow's correlation.

Boundary condition Regime	$T\,(x = 0)$ [°C]	$h\,(x = L)$ [kW m^{-2} K^{-1}]
Natural convection	$0.0579 t_{rel} + 100$	2.33
Nucleate boiling	$1.97 \cdot 10^{-5} t_{rel}^2 + 4.60 \cdot 10^{-2} t_{rel} + 108$	$0.13895(T_w - T_{sat})^2$
CHF onset	$-3.712 \cdot 10^{-2} t_{rel}^3 + 6.950 \cdot 10^{-1} t_{rel}^2 + 0.7090 t_{rel} + 226$	$h_{max,NB}(0.98\exp(t_{rel}/3.5) + 0.02)$

Discretization and temporal dependence of boundary conditions for the simulation are shown in Figure S1.2. A slight jump in the heat transfer coefficient is noticeable during the onset of nucleate boiling since the heat transfer coefficient predicted by the Rohsenow's correlation at the nucleate boiling incipience is much higher than the natural convection heat transfer coefficient. The heat transfer coefficient in the nucleate boiling regime first decreases together with surface superheat during the initial stages of the transition into nucleate boiling. Afterwards, a gradual increase with time can be observed up until CHF onset, during which the value decreases exponentially. Bottom temperature, employed as boundary condition, increases linearly within the natural convection regime and rises in accordance with a second-degree polynomial during the nucleate boiling. The bottom temperature spikes during the CHF onset as predicted by the boundary condition and observed during the measurements.

Figure S1.2. Discretization and boundary conditions for the simulation of the reference sample, where the heat transfer coefficient at the boiling surface was obtained with Rohsenow's correlation and the $T(x = 0)$ from measured data.

Figure S1.3(a) shows the temporal changes in temperature at four specific locations (boiling surface and three locations corresponding to positions of thermocouples in the sample during actual measurements). Figure S1.3(b) compares the boiling curves obtained through simulations from the values on the surface (extrapolated from the uppermost calculation node; shown in red) and the boiling curve which is calculated from temperatures at $x = 0$ and $x = 10$ mm using data reduction calculations as described within the manuscript (shown in blue). It is evident that the two boiling curves match very well and that any deviations are well within the measurement uncertainty, which is evaluated using the same procedure, described in [3], as during actual measurements (shown in green). A small difference is evident at the point of nucleate boiling incipience where the surface temperature decreases almost immediately due to a switch from constant heat transfer coefficient value to a much higher value predicted by the Rohsenow's correlation, while the extrapolated value lags slightly. However, this is caused by the implementation of boundary conditions and does not have a physical meaning. Within the nucleate boiling regime, the difference between the actual (i.e., simulated) and extrapolated value of surface temperature is less than 0.1 K as it is evident from Figure S1.3(c). Finally, the results in Figure S1.3(d) show that the difference in heat flux present on the boiling surface

(simulation result) differs very little from the heat flux measured below the surface based on the spatial temperature gradient as calculated from temperature measurements at $x = 0$ and $x = 10$ mm. The difference is one order of magnitude smaller than the heat flux measurement uncertainty and three orders of magnitude smaller than the CHF value. The heat flux change rate increases with time but remains below 1.5 kW m^{-2} s^{-1} at all times.
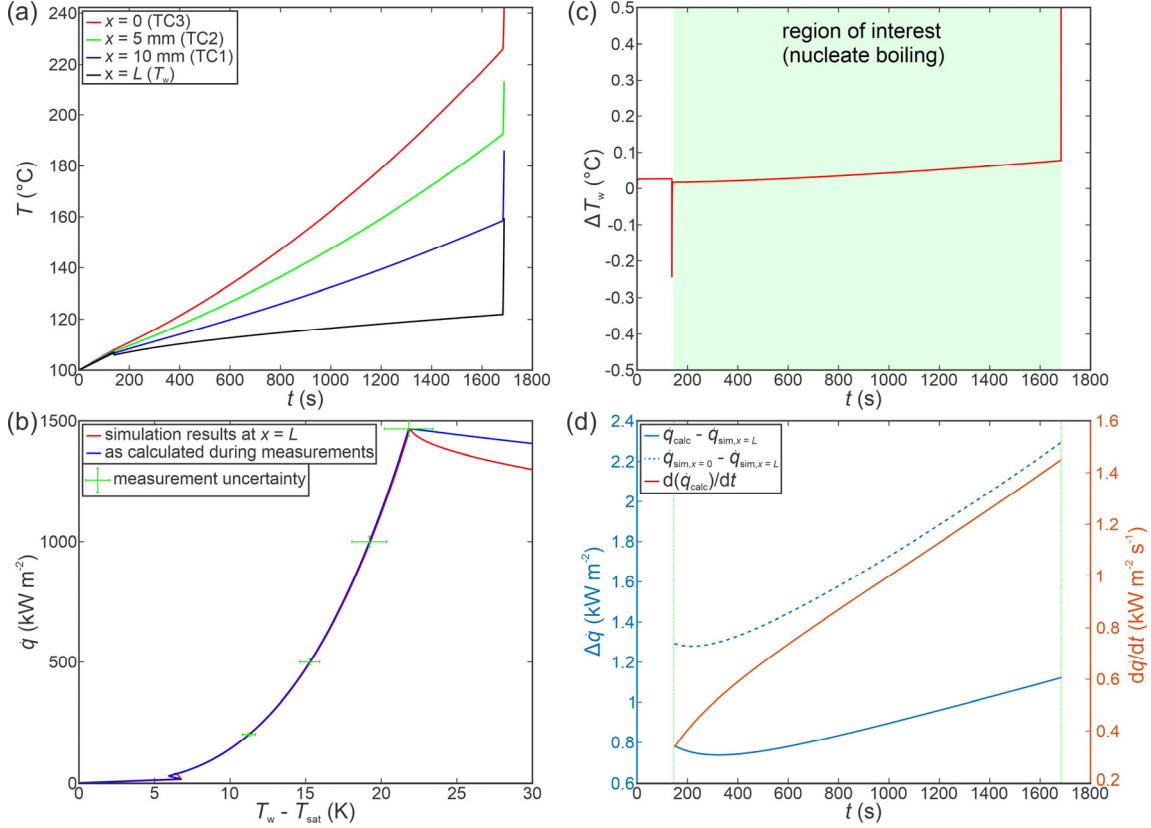
Figure S1.3. Simulation results on the reference surface using Rohsenow's correlation for nucleate boiling heat transfer coefficient. Temporal plots of temperature at four specific location (a), comparison of simulated and "as measured" boiling curves (b), difference between simulated and extrapolated surface temperature (c) and temporal change of heat flux, difference between calculated and simulated heat flux and difference between heat fluxes obtained at locations $x = 0$ and $x = L$ (d).

All of the results indicate that the dynamic measurement method with slowly increasing heat flux provides accurate results with negligible differences between the results of the simulations and values calculated using the same methodology as for experimental measurements.

Simulation on the reference sample with measured heat transfer coefficients

The second simulation was performed using the bottom temperature and values of heat transfer coefficients obtained during experiments on an untreated reference sample. The boundary conditions are summarized in Table S1.2, where t_{rel} denotes relative time within each interval (starting from zero). The exponential decay function used to model the heat transfer coefficient during the CHF onset considered the highest heat transfer coefficient obtained in the previous interval ($h_{\text{max,NB}} = 52.41$ kW m^{-2} K^{-1}). Discretization and temporal dependence of boundary conditions for the simulation are shown in Figure S1.4.
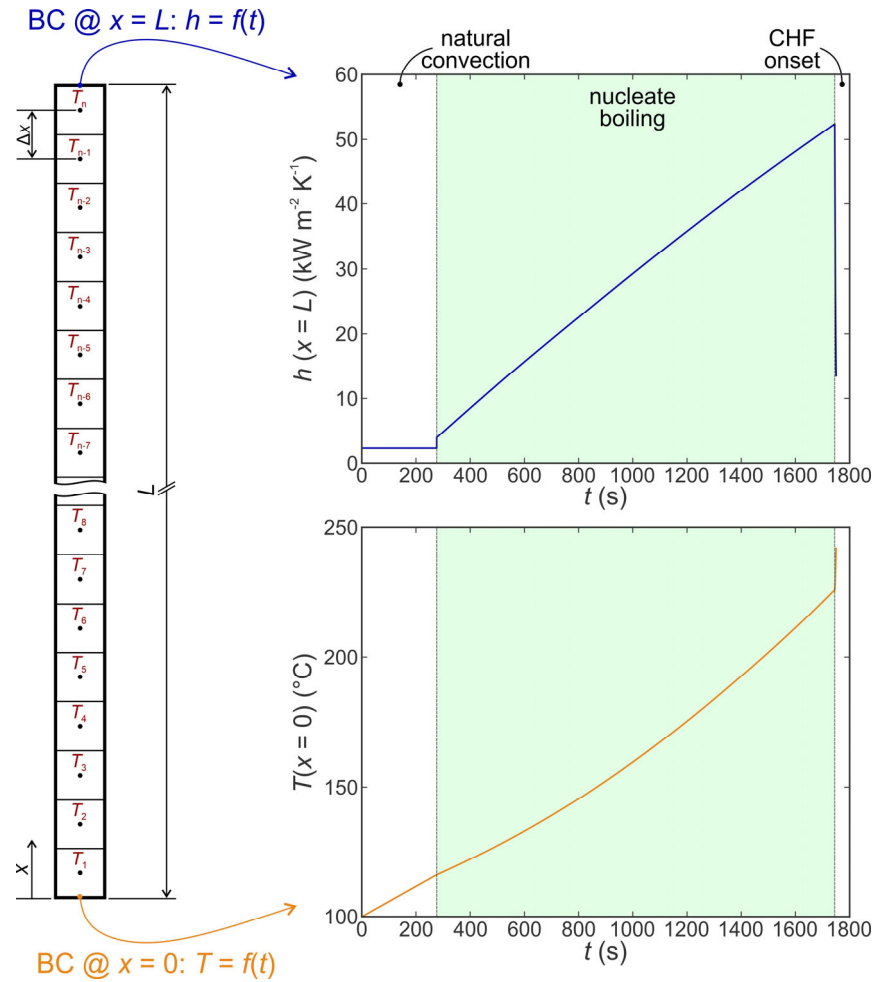

Figure S1.4. Discretization and boundary conditions for the simulation of the reference sample, where the boundary conditions for temperature $T(x = 0)$ and $h(x = L)$ were obtained from measured data.

Table S1.2. Boundary conditions for the simulation on the reference sample using measured heat transfer coefficients.

Boundary condition / Regime	$T\,(x=0)$ [°C]	$h\,(x=L)$ [kW m^{-2} K^{-1}]
Natural convection	$0.0579t_{rel} + 100$	2.33
Nucleate boiling	$1.97{\cdot}10^{-5}t_{rel}^2 + 4.60{\cdot}10^{-2}t_{rel} + 116$	$-2.68{\cdot}10^{-6}t_{rel}^2 + 3.69{\cdot}10^{-2}t_{rel} + 4$
CHF onset	$-3.712{\cdot}10^{-2}t_{rel}^3 + 6.950{\cdot}10^{-1}t_{rel}^2 + 0.7090t_{rel} + 226$	$h_{max,NB}(0.98\exp(t_{rel}/3.5) + 0.02)$

Figure S1.5(a) shows the temporal course of temperature at four specific locations, while Figure S1.5(b) compares the boiling curves obtained through simulations from the values on the surface (extrapolated from the uppermost calculation node; shown in red) and the boiling curve which is obtained from temperatures at $x = 0$ and $x = 10$ mm using data reduction calculations as described within the manuscript (shown in blue). As for the previous simulation, the two boiling curves match very well and any deviations are well within the measurement uncertainty (shown in green). Here, a small difference is also evident at the point of nucleate boiling incipience where the surface temperature decreases almost immediately due to a switch from constant heat transfer coefficient value to a higher value predicted by the boundary condition equation for the nucleate boiling regime, while the extrapolated value lags slightly. This is, again, caused by implementation of boundary conditions. Within the nucleate boiling regime, the difference between the actual (i.e., simulated) and extrapolated value of surface temperature is less than 0.1 K as evident from Figure S1.5(c). Finally, the results in Figure S1.5(d) again confirms that the difference in heat flux present on the boiling surface (simulation result) differs very little from the heat flux which is measured below the surface based on the spatial temperature gradient as recorded by temperature measurements at $x = 0$ and $x = 10$ mm. The difference is one order of magnitude smaller than the heat flux measurement uncertainty and three orders of magnitude smaller than the CHF value. The heat flux change rate increases with time but remains below 1.4 kW m^{-2} s^{-1} at all times.

These results confirm the observations from the previous simulation that the use of the dynamic method causes negligible difference between the measured values below the surface and the values that are actually present on the surface at the same moment.
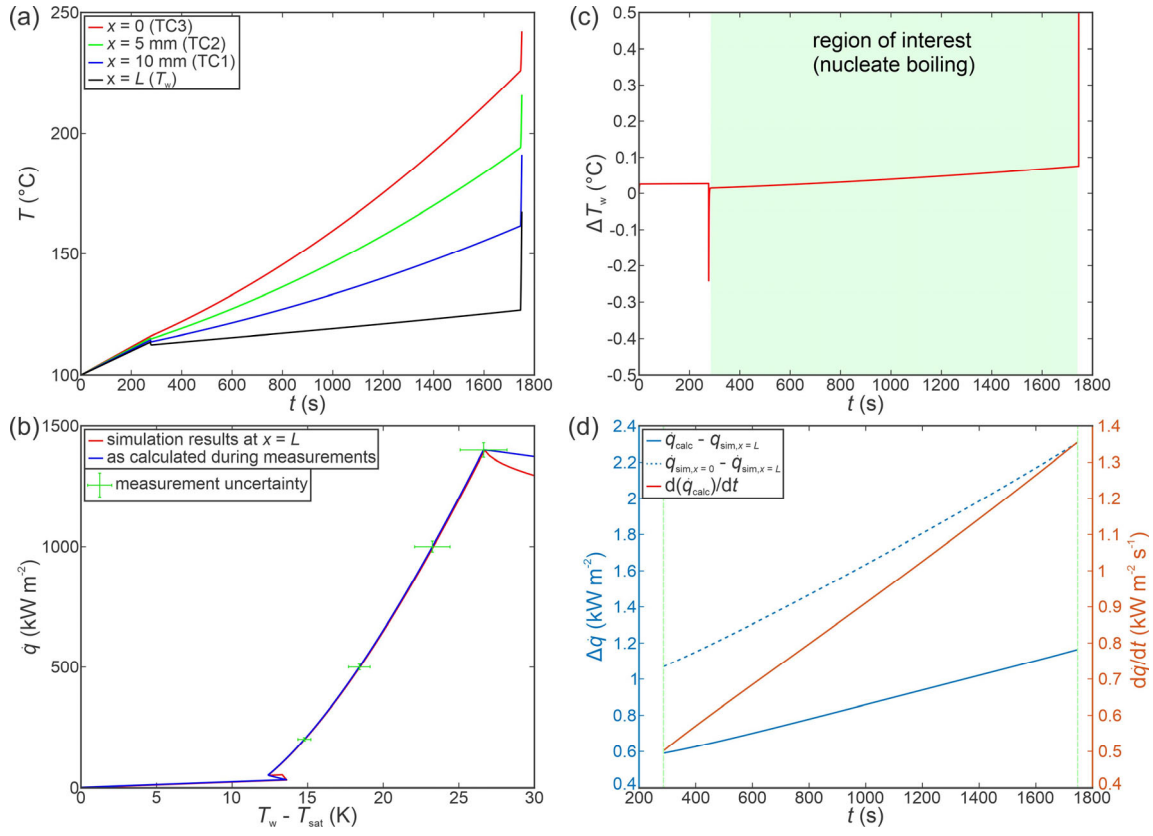
Figure S1.5. Simulation results on the reference surface using measured heat transfer coefficients. Temporal plots of temperature at four specific location (a), comparison of simulated and "as calculated" boiling curves (b), difference between simulated and extrapolated surface temperature (c) and temporal change of heat flux, difference between calculated and simulated heat flux and difference between heat fluxes obtained at locations $x = 0$ and $x = L$ (d).

Simulation on the hydrophilic A5 sample with measured heat transfer coefficients

The third simulation was performed using the bottom temperature and heat transfer coefficient data recorded during experiments on a hydrophilic sample A5, which provided the highest CHF values within this study. The boundary conditions are summarized in Table S1.3, where t_{rel} denotes relative time within each interval (starting from zero). The exponential decay function used to model the heat transfer coefficient during the CHF onset considered the highest heat transfer coefficient obtained in the previous interval ($h_{max,NB} = 138.7$ kW m^{-2} K^{-1}). Discretization and temporal dependence of boundary conditions for the simulation in question are shown in Figure S1.6.
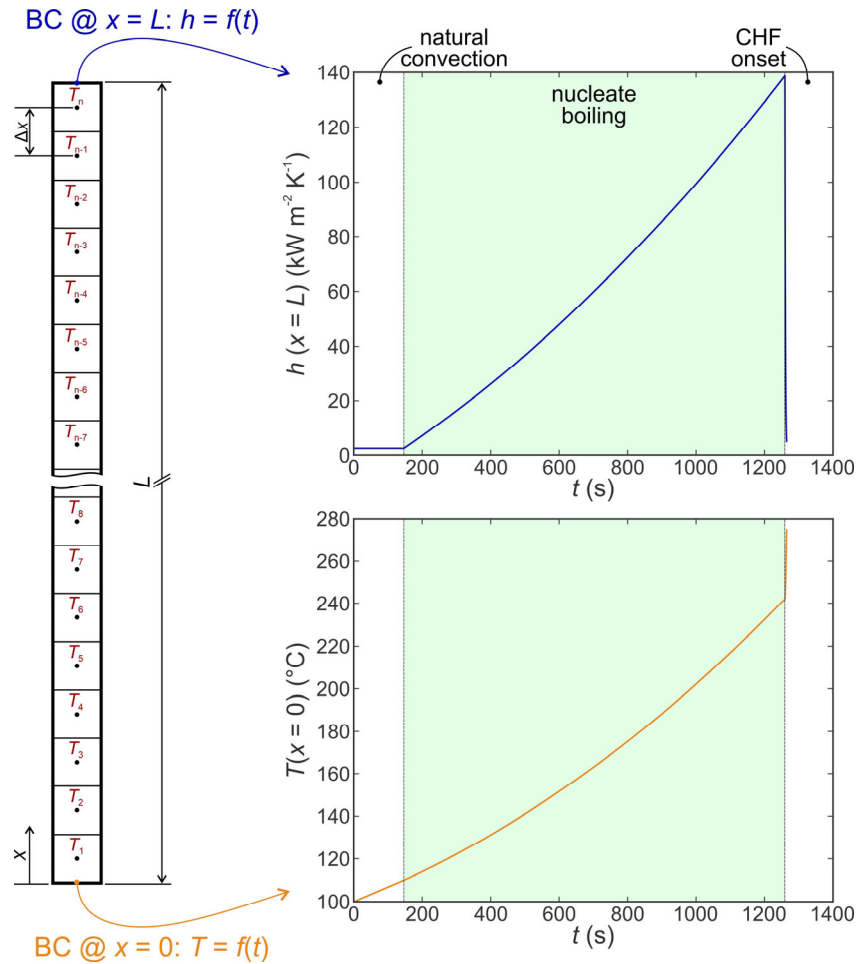
Figure S1.6. Discretization and boundary conditions for the simulation of the A5 sample, where the boundary conditions for temperature $T(x = 0)$ and $h(x = L)$ were obtained from measured data.

Table S1.3. Boundary conditions for the simulation on the A5 sample using measured heat transfer coefficients.

Boundary condition / Regime	$T\,(x = 0)$ [°C]	$h\,(x = L)$ [kW m^{-2} K^{-1}]
Natural convection	$0.0684 t_{\mathrm{rel}} + 100$	2.42
Nucleate boiling	$4.1{\cdot}10^{-5} t_{\mathrm{rel}}^2 + 7.3{\cdot}10^{-2} t_{\mathrm{rel}} + 110$	$-3.36{\cdot}10^{-5} t_{\mathrm{rel}}^2 + 8.5{\cdot}10^{-2} t_{\mathrm{rel}} + 2.42$
CHF onset	$7.2{\cdot}10^{-3} t_{\mathrm{rel}}^4 - 0.2495 t_{\mathrm{rel}}^3 + 2.3324 t_{\mathrm{rel}}^2 + 0.2242 t_{\mathrm{rel}} + 242$	$h_{\mathrm{max,NB}}(0.994\exp(t_{\mathrm{rel}}/1.4) + 0.006)$
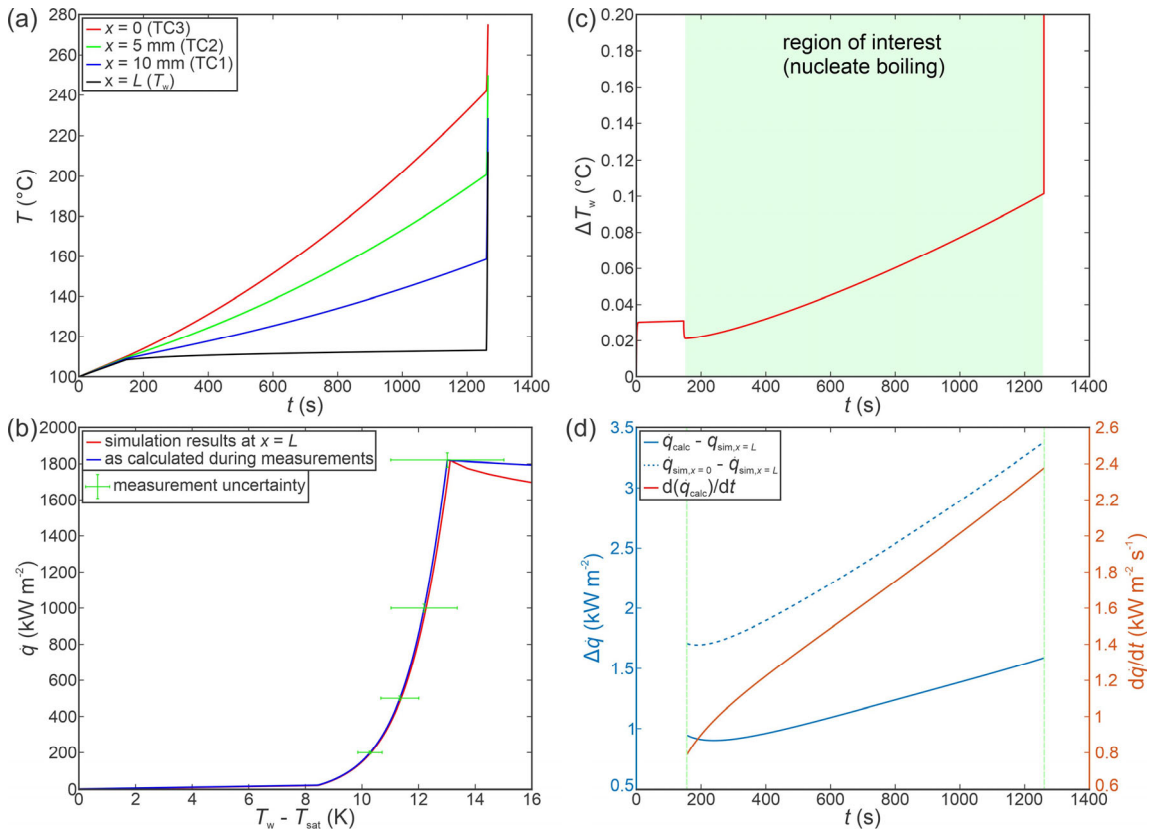
Figure S1.7. Simulation results on the A5 surface using measured heat transfer coefficients. Temporal plots of temperature at four specific location (a), comparison of simulated and "as calculated" boiling curves (b), difference between simulated and extrapolated surface temperature (c) and temporal change of heat flux, difference between calculated and simulated heat flux and difference between heat fluxes obtained at locations $x = 0$ and $x = L$ (d).

The results of the simulations on the A5 surface shown in Figure S1.7 confirm the results obtained from previous simulations. Here, the difference between the boiling curves as shown in Figure S1.7(b) is still negligible, especially when the measurement uncertainty is considered. Since no clear point of nucleate boiling was detected during the measurements, the heat transfer coefficient was modeled as continuous and hence no jump appears during the transition from

natural convection into nucleate boiling. The difference between the simulated and extrapolated surface temperature is within the same range of approx. 0.1 K for the whole nucleate boiling regime. Finally, the difference between the simulated heat flux at $x = L$ and heat flux calculated from temperatures inside the sample is below 2 kW m^{-2}. While the heat flux temporal change rate reaches approx. 2.4 kW m^{-2} s^{-1} at the end of the nucleate boiling regime, both boiling curves are still comparable and the use of dynamic measurement method on enhanced surfaces is proven to be appropriate.

Simulation on the superhydrophobic A5H sample with measured heat transfer coefficients

The final simulation was performed using the bottom temperature and heat transfer coefficient data recorded during experiments on a superhydrophobic sample A5H, which provided the highest heat transfer coefficients within this study. The boundary conditions are summarized in Table S1.4, where t_{rel} denotes relative time within each interval (starting from zero). The exponential decay function used to model the heat transfer coefficient during the CHF onset considered the highest heat transfer coefficient obtained in the previous interval ($h_{max,NB}$ = 353.8 kW m^{-2} K^{-1}). Discretization and temporal dependence of boundary conditions for the simulation in question are shown in Figure S1.8.
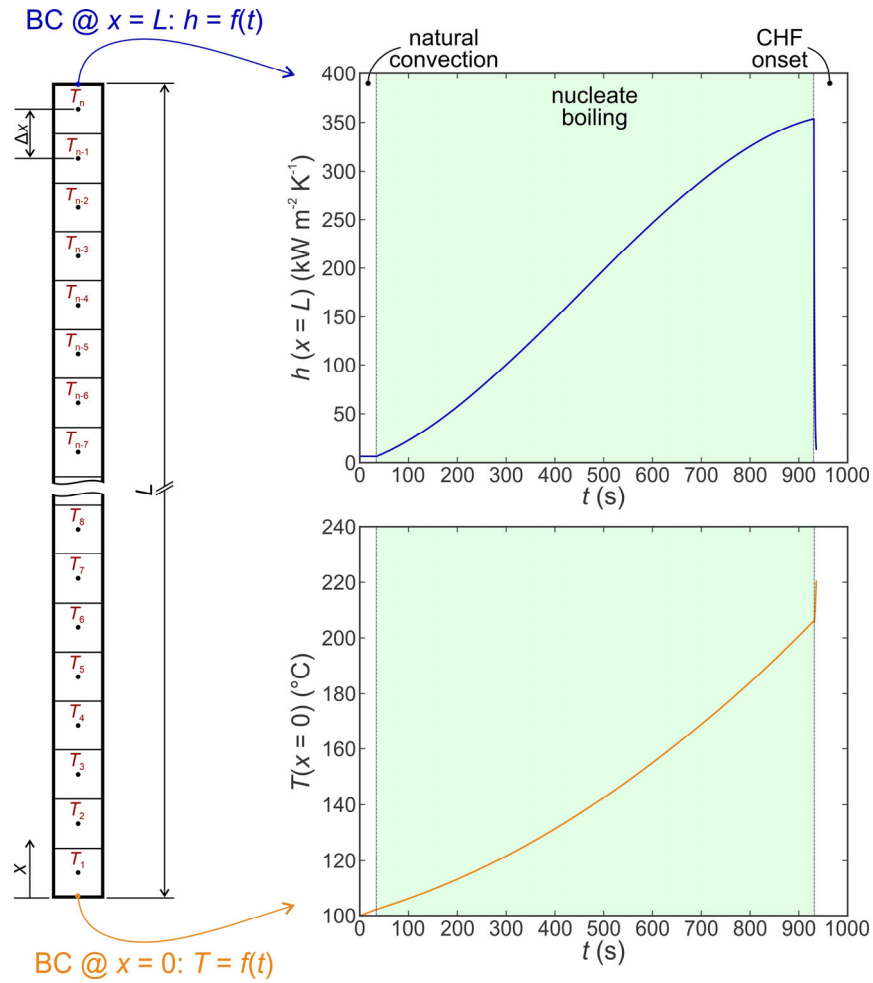
Figure S1.8. Discretization and boundary conditions for the simulation of the A5H sample, where the boundary conditions for temperature $T(x = 0)$ and $h(x = L)$ were obtained from measured data.

Table S1.4. Boundary conditions for the simulation on the A5H sample using measured heat transfer coefficients.

Boundary condition / Regime	$T\ (x = 0)$ [°C]	$h\ (x = L)$ [kW m^{-2} K^{-1}]
Natural convection	$0.0683t_{\text{rel}} + 100$	6.43
Nucleate boiling	$6.83 \cdot 10^{-5}t_{\text{rel}}^2 + 5.45 \cdot 10^{-2}t_{\text{rel}} + 102.35$	$-5.54 \cdot 10^{-7}t_{\text{rel}}^3 + 6.98 \cdot 10^{-4}t_{\text{rel}}^2$ $+ 0.207t_{\text{rel}} + 6.43$
CHF onset	$7.2 \cdot 10^{-3}t_{\text{rel}}^4 - 0.2065t_{\text{rel}}^3$ $+ 1.7966t_{\text{rel}}^2 - 1.8002t_{\text{rel}} + 206$	$h_{\text{max,NB}}(0.984\exp(t_{\text{rel}}/1.3) + 0.016)$
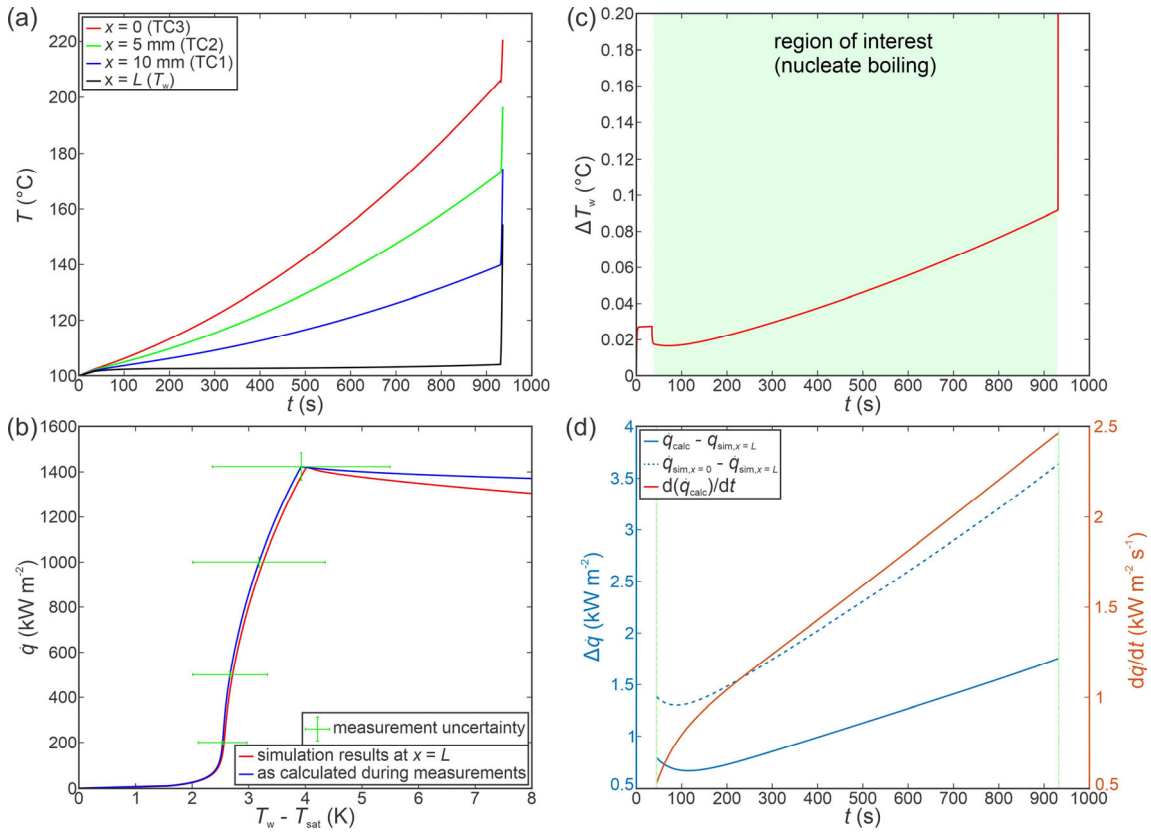
Figure S1.9. Simulation results on the A5H surface using measured heat transfer coefficients. Temporal plots of temperature at four specific location (a), comparison of simulated and "as calculated" boiling curves (b), difference between simulated and extrapolated surface temperature (c) and temporal change of heat flux, difference between calculated and simulated heat flux and difference between heat fluxes obtained at locations $x = 0$ and $x = L$ (d).

The results of the simulations on the A5H surface shown in Figure S1.9 agree with results obtained from previous simulations. The difference between the boiling curves as shown in Figure S1.9(b) appears larger than before, but the very low superheat (and the resulting stretch

of the x-axis) needs to be considered alongside the (relative) measurement uncertainty. During the measurements on the A5H surface, no clear point of nucleate boiling was detected during the measurements. As the heat transfer coefficient was modeled as continuous, no jump in values occurs during the transition from natural convection into nucleate boiling. The difference between the simulated and extrapolated surface temperature is again lower than 0.1 K within the nucleate boiling regime. Finally, the difference between the simulated heat flux at $x = L$ and heat flux calculated based on temperatures below the surface is below 2 kW m^{-2}. While the heat flux temporal change rate reaches approx. 2.5 kW m^{-2} s^{-1} at the end of the nucleate boiling regime, the boiling curves are still comparable and the use of dynamic measurement method on enhanced surfaces is proven to be suitable even for the surface exhibiting extreme boiling performance.

S2. Experimental validation of the dynamic measurement method

The accuracy of results obtained with the dynamic measurement method was also confirmed experimentally by comparing the boiling curves obtained using the dynamic method with steady-state measurements. This evaluation was performed on a copper sample (not a part of the present study), which was chemically etched in a hot alkaline solution to induce growth of CuO nanostructures, which effectively passivates the surface. A SEM image of the test surface is shown as in inset in Figure S2.1(a). First, the stability of the surface was evaluated by performing twelve consecutive dynamic runs over the course of 48 h. The results of the stability evaluation are shown in Figure S2.1(a). It is evident that small changes of the heat transfer performance are present for the first two experimental runs, but the performance then stabilizes for the last nine measurements with negligible differences between the boiling curves for runs #3-#12. Following the completion of dynamic runs, two additional test runs followed, during which steady-state measurements were performed by setting different heating powers of the cartridge heaters and averaging the results over at least 5 min after a steady state was reached. The results of these experimental runs (#13 and #14) are pairs of averaged values of surface superheat and heat flux, which are shown in Figure S2.1(b) as crosses. In the same figure, a comparison with stabilized boiling curves obtained during the last three dynamic runs is also made.
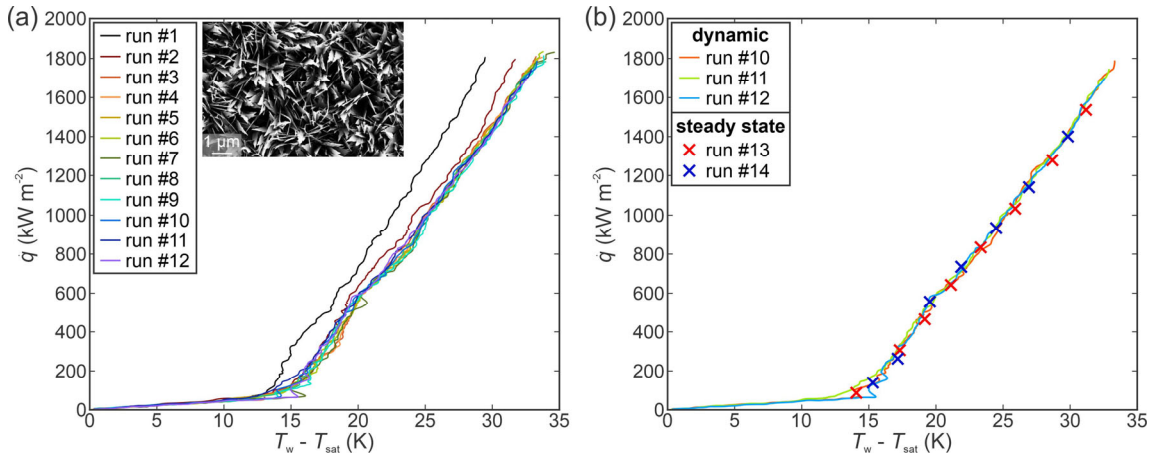
Figure S2.1. Comparison of boiling curves, obtained during 12 consecutive dynamic runs on textured copper surface (a) and comparison of last three dynamic runs (#10-#12) with the following steady-state measurements performed during runs #13 and #14 (b).

It is clearly evident from the results in Figure S2.1(b) that the steady-state measurements provide identical results to the dynamic measurements. The dynamic measurement method can therefore be used with confidence that the obtained results will not differ from the results that would be obtained using the steady-state measurement method. Furthermore, it should be pointed out that the major benefit of the dynamic measurement method is much faster

evaluation of the surface with less exposure to the boiling process, which can change the surface properties and its boiling heat transfer performance. More boiling curves can therefore be obtained on a single surface during a set period of time, which helps evaluate the stability of the surface and the repeatability of its heat transfer behavior.

References

[1]   M. Može, M. Senegačnik, P. Gregorčič, M. Hočevar, M. Zupančič, I. Golobič, Laser-Engineered Microcavity Surfaces with a Nanoscale Superhydrophobic Coating for Extreme Boiling Performance, ACS Appl. Mater. Interfaces. 12 (2020) 24419–24431. https://doi.org/10.1021/acsami.0c01594.

[2]   W.M. Rohsenow, A method of correlating heat transfer data for surface boiling of liquids, Trans. ASME. 74 (1952) 969–976.

[3]   M. Može, M. Zupančič, I. Golobič, Investigation of the scatter in reported pool boiling CHF measurements including analysis of heat flux and measurement uncertainty evaluation methodology, Appl. Therm. Eng. 169 (2020). https://doi.org/10.1016/j.applthermaleng.2020.114938.